On the effect of sediment composition and concentration on suspended sediment measurements in a lab setting

J.F.D. Lammers

January 10, 2023

MSc thesis

Hydrology and Quantitative Water Management Group
Wageningen University

There is no education like adversity
Benjamin Disraeli

Abstract

Ultrasonic profilers, calibrated with optical in situ suspended sediment concentration (SSC) sampling are used to determine SSC in rivers and laboratories in a non intrusive manner with a high spatiotemporal resolution. In this report flaws of the UB-Lab 2C (UBT) and LISST in a recent flume experiment with sand and silt are expounded in order to advice on future research.

The optical SSC measuring device, LISST, was not able to record reasonable data due to the milky white state of the water once silt was added to the bed mixture. For the experiments without silt, residual clay content from previous research decreased the transmission value below the threshold. These two factors caused the serious underestimation of SSC values for silt experiments and creation of SSC distortion for the majority of the sand experiments.

In the assessment of a transmission threshold decrease from 0.1 to 0.05 - with the eventual goal to use more of the recorded data - it became evident that this threshold decrease would not lead to the aimed result. Data of the lowered threshold contained more noise and were biased. Therefore, the transmission threshold should not be lower than 0.1.

The UBT a methodological flaw. The backscatter amplitude of this acoustic velocity profiler dropped significantly once medium silt was added to the bed. The acoustic attenuation is attributed to the viscous absorption from the fine particles.

The suspended sediment transport flux calculated from a valid backscatter-suspended sediment concentration relation shows some confidence. Only near the bed, the transport flux exceeds physical limitations.

Suggestions for experimental setup adjustments to improve the data acquisition are to calibrate the data at two depths in order to account for the attenuation, decrease the LISST laser path length or dilute the SSC samples. This way the relation between suspended sediment content and backscatter amplitude can accurately be derived for sand and silt.

Contents

1 Introduction

Sediment transport is a convoluted subject, with many processes acting at the same time. Understanding sediment transport however, is key in many river managing issues, such as maintaining harbours navigable.

In order to measure suspended sediment transport in rivers, solid methods need to be derived. Many procedures have been developed over time, each with their own dilemma.

On the basis was manually sampling and analysing the suspended sediment concentration (SSC) and particle size distribution (PSD) by dry weighing the sample or through gravimetric analysis in a laboratory (Edwars & Glysson, 1999; Davis, 2005; Gray et al., 2008). This process is extremely time consuming, costly, in some accounts risky and only provides low temporal and spatial resolution suspended sediment content.

Once laser transmission and diffraction sediment samplers became commercially available, SSC and PSD data collection became less time consuming and the recordings were continuous. The laser diffraction devices were auspiciously used in many marine and estuarine environments (Agrawal & Pottsmith, 1994, 2000; Agrawal & Traykovski, 2001; Gartner et al., 2001; Mikkelsen & Pejrup, 2000, 2001). The only measuring issue is the low spatial resolution. These laser-based devices can only sample a single point. This implies that collection of instantaneous suspended sediment content profiles are not possible (Agrawal & Pottsmith, 2000; Agrawal et al., 2008) unless multiple devices are installed above each other. This proposed setup hampers flow. These extraordinary induced flow properties can cause additional sediment suspension, creating bias in suspended sediment content determination.

This flaw in optical measurement was one of the reasons the scientific world turned to alternative SSC data collection techniques with a less intrusive manner. Acoustic backscatter is a good proxy for SSC determination. Initially, acoustic devices utilized Doppler shift to determine the flow velocity of the entire water column. However, from the already acquired backscatter data, some degree of suspended sediment content could be deduced.

The method of monitoring suspended sediment from acoustic backscatter has successfully been adapted in fundamental laboratory studies as well. Betteridge et al. (2008) determined the suspended sediment content of glass beads. This relation can fundamentally be applied to all types of sediments to establish sediment transport relations, including mixtures of fine sediments.

There are, however, still some pitfalls that need further clarification in order to determine SSC correctly. In a laboratory experiment from April until August 2022 at Wageningen University and Research, several bed mixtures of sand and silt were assessed on sediment transport properties. The aim was to determine for each sand-silt mixture a suspended transport relation in order to examine the effect of silt content on bed stability and suspended transport. Lab experiments offer controlled environments, suitable for systematic measurement and manual adjustments of the circumstances, and have been performed in many occasions (van Ledden et al., 2004; Van Rijn, 2020; Bartzke et al., 2013; Baas et al., 2013; Naqshband et al., 2016; Naqshband & Hoitink, 2020). However, due to unforeseen circumstances, multiple problems arose in the obtained data. Once silt was added, the devices recorded suspended sediment content and backscatter amplitudes opposite or attenuated to what was expected from the observations (milky white water). Also in experimental runs with sand, SSC values were distorted. Therefore, the scope of this research is to find out what the effect of sediment mixtures are on the devices in order to prevent similar problems to arise in future research.

Another topic of interest for this research is the minimal transmission value. Sequoia Scientific (2022) provided a threshold transmission value of 0.1, indicating that from the emitted beam a fraction of 0.1 is observed. Turbidity and laser path length through the medium decrease the transmission value. This threshold indicates the maximum observable SSC (see section 2.1.2 for a detailed overview). Thus, lowering the threshold would lead to larger range of SSC determination. Sequoia Scientific (2022) does not specify the reasoning behind designating the threshold value to be 0.1. In order to increase the data availability, this thesis focuses on the effect of lowering the transmission threshold on SSC data quality as well. When lower transmission values provide acceptable SSC data, more knowledge about turbid waters can be acquired with the same setup.

1.1 Research objective

Determine the effect of sediment composition and concentration on suspended sediment content measurements in a lab setting. To reach this goal the following research question is formulated:

What is the effect of sediment composition and suspended sediment concentration on suspended sediment transport determination in a lab setting?

The following two sub-research questions are asked to guide the main research question:

- What is the effect of sediment composition and suspended sediment concentration on backscatter measurements?
- What is the effect of sediment composition and suspended sediment concentration on optical suspended sediment measurements?

In addition, to further understand the limits of the LISST, this research aims to find the minimum transmission value before the SSC data become unreliable. Decreasing the transmission threshold would lead to a higher data availability. The following question is added to the research:

What is the effect of lowering the transmission threshold from 0.1 to 0.05 on SSC data quality?

2 | Theoretical background measuring devices and sediment concentration - backscatter relation

In order to fully grasp the potential of acoustics in spatiotemporal suspended sediment transport management and data acquisition, in this chapter the process in optical data acquirement for the LISST will be covered first. The succeeding paragraph goes into detail how the UBT operates and from which processes the flow velocity profiles and suspended sediment concentrations are extracted. At last, the relation between the backscatter amplitude and suspended sediment concentration will be discussed.

2.1 Optics

2.1.1 LISST principles

The Laser In-Situ Scattering and Transmissiometer (LISST) is a laser diffraction particle size analyser which can be fully submerged in water. This device measures the in situ grain size distribution and corresponding concentrations in a point at a sampling frequency of 1 Hz (Sequoia Scientific, 2022).

Figure 2.1 shows the measurement principle of the LISST. The red line indicates the laser path through the opening where water passes. The sediments in the water scatter the laser (i.e. the laser is diverged when hitting a sediment particle). After passing lenses, the scattered laser is projected on the focal plane at a certain distance from the central axis. The distance from this axis corresponds to a certain grain size [μm]. The intensity of the scattered beam on the focal plane corresponds to the concentration [$\frac{\mu l}{l}$]. The distance from the central axis to the focal plane is inverse to the grain size. The grain sizes are measured from 1 to 500 µm in a evenly logarithmic distribution of 36 bins.
Suspended particles larger or smaller than the given PSD range are not omitted, these concentrations are added to the largest and smallest grain size concentration to size accordingly. The overestimated suspended sediment concentration occurs in the tails of the PSD (Agrawal & Pottsmith, 2000; Agrawal & Traykovski, 2001; Mikkelsen et al., 2005; Reynolds et al., 2010; Andrews et al., 2011).

Table 2.1: The maximal observable SSC ($\frac{\mu l}{l}$) for each grain size for an optical path length of 25 mm and a transmission of 0.3 and 0.1

Mean particle diameter (μm)	Wentworth grades	SSC max t=0.3 ($\frac{\mu l}{l}$)	SSC max t=0.1 ($\frac{\mu l}{l}$)
1.95	Clay	31	159
3.9	Very Fine Silt	63	318
7.8	Fine Silt	125	636
15.6	Medium Silt	251	1272
31.25	Coarse Silt	502	2547
62.5	Very Fine Sand	1029	5094
125	Fine Sand	2010	10188
250	Medium Sand	4020	20377

To omit the effect of ambient light on the receiver, the external light is directly measured by the LISST and subtracted from all the light reaching the observation.

2.1.2 Maximum observable SSC

Like any other optical device, the LISST has an observation limit for suspended sediment concentration. The laser cannot reach the optical sensor when the water is too turbid. This concentration limit depends on many factors among which particle size is an important variable. The maximal observable SSC (SSC_{max}) is derived by Agrawal et al. (2008):

$$SSC_{max} = \frac{-d\ln(t)}{1.13L} \tag{2.1}$$

t Is the optical transmission, this value must be between 0.3 and 0.9 for high quality SSC recording (Sequoia Scientific, 2022), L is the path length [m] (25 mm for the LISST-200X) and d represents the mean particle size [μm]. The maximal observable SSC for the range of sediments (table 2.1 with transmissions of 0.3 and 0.1) increases with grain size.
Sequoia Scientific (2022) proposes the transmission to be between 0.9 and 0.3 for high quality SSC recordings, however, keep the absolute minimum at 0.1. Once the transmission drops below this point, the data is invalid according to Sequoia Scientific (2022). It is unclear what the reason is for the threshold to be set to 0.1.

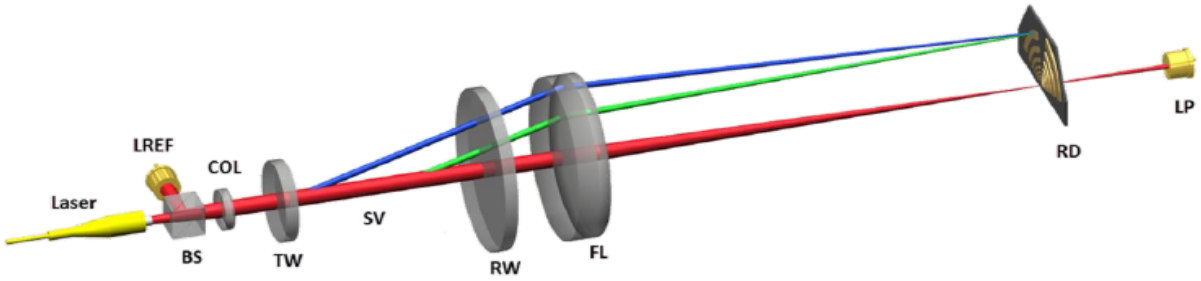

Figure 2.1: An illustration of the LISST measurement principle. The laser is scattered on the RD plane into 36 grain size bins and 36 concentration bins. After Sequoia Scientific (2022)

2.2 Acoustics

2.2.1 UBT principles

The UB-Lab 2C is an acoustic current profiler developed by UBERTONE for commercial usage. Similar to other renowned acoustic current or velocity profilers (RD instruments, Nortek, SonTek), the UB-Lab 2C emits ultrasonic acoustic waves and computes the flow velocities at multiple depths below the transducer from the returning wave. Depending on the setup, either a 2 dimensional profile or a 3 dimensional profile can be produced. The standard 2C setup is composed of one emitter (T_0) and two receivers (T_1 and T_2) (figure 2.2). The 3C extension are two receivers, orthogonally installed to the 2C receivers. These two transducer couples do not measure the velocity - and backscatter (Sv) profiles at the same moment, as the measurement of Tr_1 and Tr_2 needs to be finished before Tr_3 and Tr_4 start. Average 3D profiles can be derived from the 3C setup. However, due to the measurement principle of singly measuring each component, instantaneous profiles do not show the same turbulent whirls in streamwise and lateral direction.

For clarity and convenience, in further paragraphs a 2C setup will be used as an example to explain the UBT functioning.

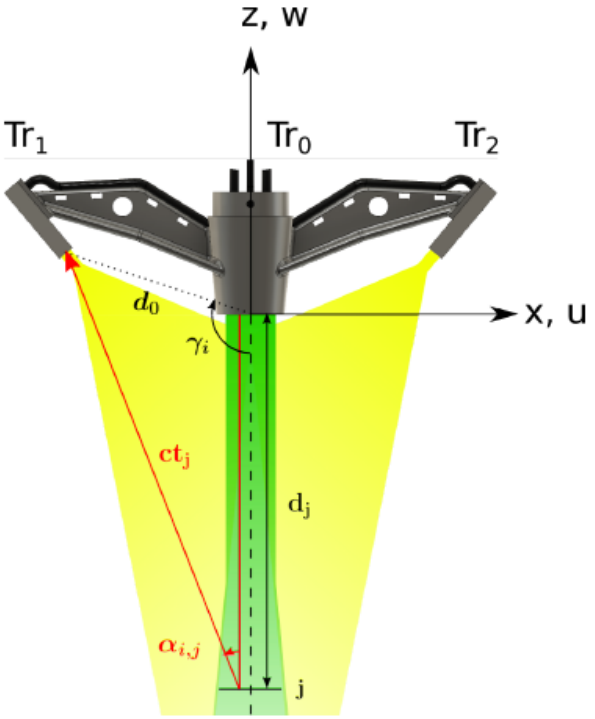

Figure 2.2: The cylinder-cone shaped acoustic beam in which velocity and backscatter data is collected in various cells. Subscript j denotes the physical units at cell j. (from UBERTONE (2019))

2.2.2 Acoustic velocity principles

If the emitted wave path crosses a moving medium, the returning wave has a shifted frequency proportional to the flow velocity. This phenomenon is first explained by Doppler (1842), whereafter this frequency shift is named the Doppler shift.

The UBT emits ultrasonic sound waves from the middle transducer down the central axis of the UBT (figure 2.2). This axis and the axis following transducer 1 to 2 are internally used as the reference coordinate system (x-z) in which the velocities (u and w) are eventually derived. After emission from Tr_0 and reflection by the medium, the reflected sounds are received at Tr_1 and Tr_2. The transducer holder and device are designed such that the velocity and backscatter data can be accurately collected up to a depth of 0.4 metres from Tr_0.

The sampling volume (green area in figure 2.2) has the shape of a cylinder in the first few centimetres, whereafter a diverging cone emerges. The cylinder-conical shape is the product of the Rayleigh integral, used to minimise the energy losses and side lobe strength. The length of the cylindrical part ($1.6 * x_{Nf}$)

is defined by the Fresnel equation:

$$x_{Nf} = \frac{R_T^2 f_0}{c} \tag{2.2}$$

x_{Nf} [mm], R_T [cm], f_0 [MHz] and c [m/s] are the near field distance, transducer surface radius, emission frequency and speed of sound in water respectively. The acoustic cylinder has the same radius as the Tr_0.

The Fraunhofer equation defines the conical spread as the 'upper to half angle', Θ [°]. The spread is derived from the following equation:

$$\Theta = \frac{0.61c}{R_T f_0} \tag{2.3}$$

So, these two combined produce the cylinder-cone shape at which the cone develops at 1.6 times the near field distance. Inside this cylinder-cone model, 90 percent of all energy emitted by the transducer is contained (Fischer, 2004).

To measure the velocity at multiple depths, the transducer emits a burst of multiple pulses. Echoes of the emitted waves scatter in all directions among which the direction of the receiving transducers. The observation cell is between the upper and lower boundary of it, which position is determined through:

$$d_j = \frac{d_0^2 - ct_j^2}{2(d_0 cos(\gamma) - ct_j)} \tag{2.4}$$

c is the speed of sound through water [m/s] and t_j [s] is the time between emit at Tr_0 and receipt at $Tr_{1,2}$ via cell j. Thus, ct_j denotes the traveled path of the sound from the emitter via cell j to the receiver in metres. d_0 [m] is the flying distance between Tr_0 and Tr_1 or Tr_2. γ represents the fixed angle between the beam axis and d_0 axis [°] (figure 2.3).

2.2.3 Phase coding

Transducers 1 and 2 receive a mix of echoes from multiple pulses at the same moment originating from different depths. So, to determine the velocity at the correct depth at the correct moment, coded pulses are emitted which can in terms of echoes only correspond for at one moment for only one depth. An observed delay of this same echo means it is reflected at larger distance. Now the velocities at different depths at the same moment for multiple moments are obtained, instantaneous velocity profiles are derived.

Another reason for using coded pulses is to omit any external noises (pump vibration, flume vibration, etc.)

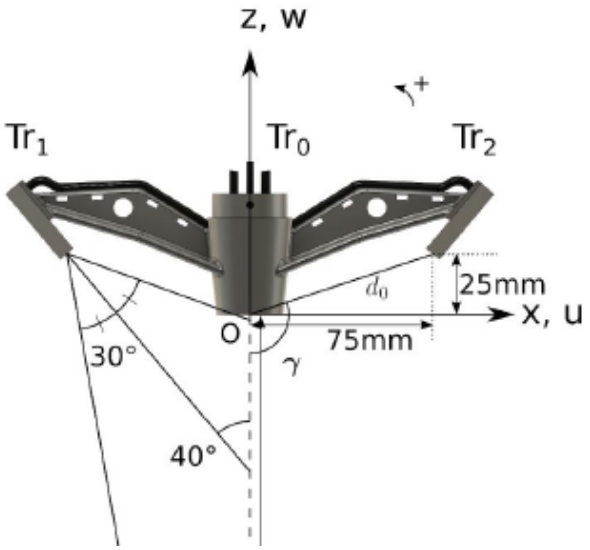

Figure 2.3: A detailed overview of the transducer geometry (UBERTONE, 2019)

and ghost echoes. These ghost echoes occur in confined volumes and can be interpreted as Doppler shifted frequencies creating bias, thus, incorrect velocities (UBERTONE, 2019).

2.2.4 Profile sampling rate

Previously discussed, from a number of coded pulses (n_{ech}) one instantaneous profile is made. One profile repetition salvo is fired at a certain frequency to prevent older echoes to influence the measurement, this is the Pulse Repetition Frequency (PRF) [Hz]. The sampling rate of instantaneous profile acquisition is:

$$f_{aq} = \frac{PRF}{n_{ech}} \tag{2.5}$$

The number of samples/coded pulses (n_{ech}) should be at least 30 to achieve good quality of an instantaneous profile. The PRF also defines the exploration depth as the bundle of pulses must have returned before a new bundle can be emitted. According to the Nyquist-Shannon theorem (Shannon, 1949), the interval between two pulses for Doppler shift (f_d) determination must be between $\pm\frac{PRF}{2}$. If this condition is not met, the received echoes are sampled with a phase jump creating bias in velocity determination.

2.2.5 Velocity range

The Doppler shift is measured for each cell by both transducers Tr_i, however, because the flow from one transducer to the other the observed frequency shift ($f_{i,j}$) is proportionally opposite.

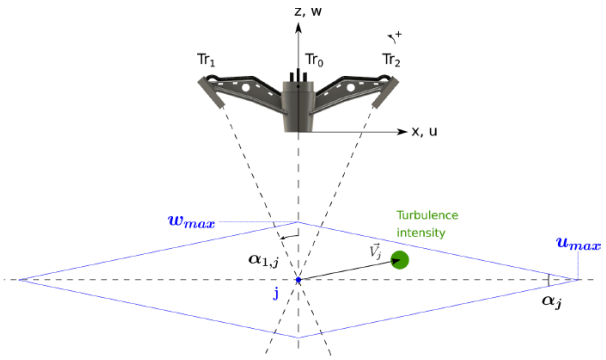

Figure 2.4: In blue the observation diamond. The dimensions of the diamond depend on distance from the transducers. The velocity vector V_j must be within the diamond (UBERTONE, 2019).

Visible in figure 2.4 is the dependency of the maximum observable velocity vector ($V_{j,max}$) on the angle between the central axis and receiver axis α_j. The velocity vector is the product of the observed velocities in x and z direction, it is the vector the UBT observes and needs to be within the observable range. $u_{max,j}$ increases with a decreasing central-transducer axis angle α_j. This decrease of axis angle comes from the distance between the transducers ($d_{(Tr_0-Tr_1)} = 75$ mm) and the observed cell (d_j). w_{max} however, decreases with depth as an decreasing angle. w_{max} does not drop as much as the u_{max} increases. The x and z velocity components are calculated from equations 2.6 and 2.7:

$$u_j = \frac{V_{2,j} - V_{1,j}}{2sin(\alpha_j)} \tag{2.6}$$

$$w_j = \frac{V_{1,j} + V_{2,j}}{2(1 + cos(\alpha_j))} \tag{2.7}$$

u_j and w_j are the velocities [m/s] in streamwise and upward direction at cell j and $V_{1,j}$ and $V_{2,j}$ [m/s] are the observed velocity vectors by transducers 1 and 2 at cell j. The denominator is a correction factor. Once the angle (α_j) becomes too small, large measurement errors occur. These errors can be up to a factor 2.88 at 0.4 metres below the transducers. This adds up to the reason UBERTONE (2019) set the exploration depth limit to 40 centimetres.

From the settings and the maximum observable velocity dependency on depth, a maximal observable velocity range per depth is automatically produced on the UBT interface. When conducting an experiment, the expected field velocities should be within the range or the echoes are interpreted incorrectly.

2.2.6 Backscatter amplitude

The UBT expresses the received backscatter energy in terms of amplitude [Volts]. The backscatter amplitude attenuates over depth as water and sediments dissipate the emitted energy. Sediments also have the property to scatter the incoming sound into different directions, therefore, dissipating the energy. This prevents sound to travel deeper into the water column. However, the backscatter intensity received from this sediment is very high. In order to combat the backscatter attenuation to produce a complete backscatter profile, the UBT is provided with a gain function:

$$G_{dB} = a_0 + a_1 ct_j \tag{2.8}$$

The gain (G_{dB}) is assumed constant along the profile ($a_1 = 0$) and this gain is preserved for all experiments.

2.3 Sv-SSC relation

The received backscatter intensity depends on the amount of sediments in suspension. As an example to explain the backscatter-SSC relation, imagine yourself talking into the vast emptiness of a windless sky, you barely hear your echo coming back. If you however, put some layers of wire fence in front of you, you receive some backscatter. Now, you see that the wire density of the netting and number of nettings behind each other determine the backscatter intensity. You can determine the number of nettings from the backscatter and a sample of the wire density. What would happen if the wire shape changes? If the wire is perfectly round, the incoming acoustic wave is dispersed in all directions. However, when the wire is more edged there is a backscatter direction preference. Depending on this preference direction, you might perceive yourself more or less loud.
Let us continue the thought experiment keeping the UBT measuring principle of emit-receipt time, cell distance and profiling in our mind. If you want to profile the number of fences behind each other, you need the backscatter from the last fence at least to reach you. However, the emitted sound is reflected in different directions by each wire, therefore dissipating the intensity. This dissipation can be dealt with through either a Gain function like UBERTONE (2019) proposed or through calibrating the fence number close to you and at the end with the backscatter from these distances. The latter is more accurate as it continuously samples both the at-

tenuated backscatter profile and the corresponding fence number at two locations, while the Gain function is a simplification based on only one parameter. This same process has been practiced by many researches to monitor the SSC through the backscatter intensity and SSC sampling for calibration (Sassi et al., 2012; Heus, 2020; Hoitink et al., 2017).

Recording the backscatter intensity near the surface and near the bed accounts for the attenuation caused by the water and sediments. Then, the backscatter intensity and measured SSC are regressed to obtain a function that can determine the suspended sediment content of an entire column based upon the recorded backscatter profile. A simple, yet effective first order relation between SSC and the backscatter (S_v) is a logarithmic relation (Urick, 1983):

$$Sv = a\log(SSC) + b \tag{2.9}$$

which can be rewritten to:

$$SSC = 10^{(aSSC)} * B \tag{2.10}$$

10^b is substituted for B.

This formula is the foundation of SSC profiling and SSC flux determination in presented research.

3 | Methods

3.1 Experimental setup

The experiments were conducted in the Kraijenhoff van de Leur Laboratory for Water- and Sediment dynamics, part of Wageningen University. The setup is displayed in figure 3.1. The experimental setup was allocated in the tilting flume. This is a unidirectional water flume; 14.4 metres in effective test reach length, 1.2 metres wide and has a maximum depth of 50 centimetres. For the experimental runs, the tilting angle of the flume was set at 0.01° to represent delta conditions. The flume is filled with a 10 centimetre high sediment bed, over which 15 cm of fresh water flows. These sediments were systematically altered to create different sediment bed mixtures. To maintain the same water depth for different discharges, the water level was adjusted by a weir at the end of the flume. To measure the flow velocity- and backscatter profile, an UB Lab-2C was installed near the end of the flume. Furthermore, a Laser in Situ Scattering and Transmissometer (*LISST*) was fixed 1.1 metres behind the UB Lab-2C to observe the suspended sediment concentration of the water simultaneously. An important note to make is that this does not imply the same water volume passes both the UBT and LISST, it merely suggests that over a longer period of time approximately the same content has passed both observers.

3.2 Experimental runs

As discussed above, different currents are imposed over the sediment bed. To clarify the exact procedure, the terms *Set*, *Experiment* and *Run* need some explanation.

A *run* is a single experimental run with one discharge and one bed composition. The measurement cycle of one run takes 15 minutes while the length of an entire run to reach equilibrium state depends on the discharge. Equilibrium times found by Baas (1994) and Naqshband et al. (2016) for certain discharges were used as minima. The used equilibrium times are given in table 3.2. Multiple runs with the same bed composition (eg. 10% silt 90% fine sand) but varying discharges ranging from 30 to 100 litres are called an *experiment*. These runs are in order of increasing discharge. The sediments used in a *set* are the same but in different proportions (*experiments*). Thus, this entire lab experiment is composed of 3 sets, individual sets consist of multiple experiments with multiple runs each. Table 3.1 shows all sediment compositions utilized.

Table 3.1: The composition of every run in mass fraction [-] per component. S1 means the experiments with medium and fine sand and S2 means the experiments with medium sand and coarse silt. S3 encompasses the experiments with medium sand and medium silt.

Code name	Medium sand	Fine sand	Coarse silt	Medium silt
S1_E1	0	1	0	0
S1_E2	0.18	0.82	0	0
S1_E3	0.35	0.65	0	0
S1_E4	0.49	0.51	0	0
S1_E5	0.65	0.35	0	0
S2_E1	1	0	0	0
S2_E2	0.98	0	0.02	0
S2_E3	0.95	0	0.05	0
S2_E4	0.9	0	0.1	0
S2_E5	0.8	0	0.2	0
S2_E6	0.7	0	0.3	0
S2_E7	0.5	0	0.5	0
S3_E1	0.98	0	0	0.02
S3_E2	0.97	0	0	0.03
S3_E3	0.91	0	0	0.09
S3_E4	0.77	0	0	0.23
S3_E5	0.7	0	0	0.3

For this research, a few specific bed compositions are chosen based upon threshold values found in literature. Bartzke et al. (2013) found the stabilizing properties of non-cohesive silt in a sand-silt bed to arise at low bed silt of 0.18 mass percentage. Therefore, for both the coarse and medium silt an initial threshold of 2.0% silt mass was set to determine the effect of low silt content. Next, larger steps in silt content addition were taken, until the mass percentage silt reached 50% or 30%.

In a study of Yao et al. (2022), the erosive behaviour of non-cohesive silt was categorised in sand-like or clay-like. They found a threshold silt content of 35% separated the two regimes. To see whether this is also valid for our experiment in case of course silt, silt content of 30% and 50% were assessed.

For each discharge used in this experiment, the calculated flow velocity, uniform with depth, is denoted in table 3.2.

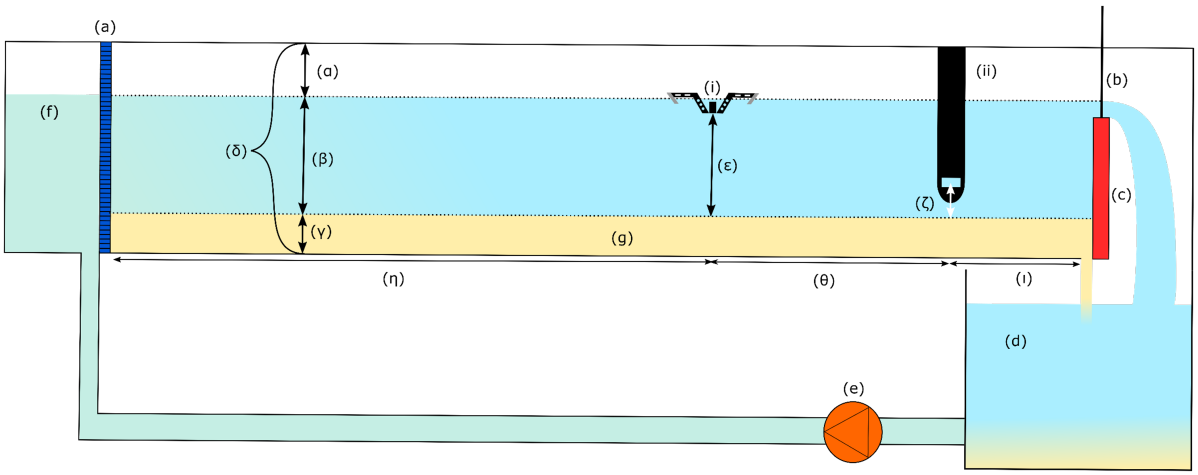

Figure 3.1: Flume setup: (a) flume inlet; (b) outlet; (c) adjustable end gate; (d) outlet basin; (e) pump; (f) inlet basin; (g) sediment bed; (i) UBT Lab-2C; (ii) LISST-200X; (α) 25 cm; (β) water column, 15 cm; (γ) sediment column, 10 cm; (δ) 50 cm; (ϵ) transducer distance to bed, 8 cm; (ζ) distance LISST sampling volume to bed, 6 cm; (η) distance space between inlet and UB Lab-2C, 11 metres; (θ) distance between the UB Lab-2C and the LISST, 1.1 metres; (ι) distance between LISST and outlet, 2.3 metres; (Note, this figure is not on scale)

Table 3.2: Discharges, corresponding uniform flow velocities and the minimal length of each run to reach equilibrium state based on work of Naqshband et al. (2016) and Baas (1994)

Q (l/s)	v (m/s)	Min. run time (h)
30	0.25	0.5
45	0.38	10
60	0.5	0.5
80	0.67	5
100	0.83	5

3.3 Data analysis

3.3.1 Data filtering

LISST

First of all, LISST data were filtered on outliers with the 95 percentile rule. Prolonged elevated backscatter data were not filtered out as it represents sediment whirls. These elevated values were not as high as the outliers. The outliers occurred sporadically and had a very short longevity. Therefore, it was easy to filter out any outliers.

When the instantaneous Particle Size Distributions (PSDs) of one run are merged together in one figure, (eg. figure 4.1) the general PSD of the LISST observation for that certain run becomes evident, but also the deviations that are observed within one run. Noticeable are the open endings of the PSDs at grain sizes smaller than 1.2 µm and larger than 480 µm. The bed material does not contain any clay material, only silt with grain sizes larger than 2 µm (table A.1 and figure A.1). Nor do the sediment beds contain sand grains larger than 330 µm. Therefore, the PSDs are snipped at 2 and 330 µm and further analyses are conducted without the concentration of the aforementioned particle sizes.

UBT

Similar to the initial filter on the UBT data, the LISST recorded SSC data were filtered on the 95 percentile rule. Again, outlier peaks were distinctively different than valid high concentrations.

3.3.2 Data processing

The LISST samples every second the SSC with the corresponding grain size distribution in a sample length of 25 mm (Sequoia Scientific, 2022). The UBT however, samples a profile in 0.16 seconds (6.25 profiles per second). Each bin (*a bin is a cell in the profile*) is approximately 1.5 mm high. The user can alter the sampling frequency if more or less spatial or temporal resolution suited for the specified research (UBERTONE, 2019).

For the backscatter - suspended sediment concentration relation, the SSC recorded by the LISST is averaged over the entire period of time the LISST and UBT data time overlaps. Similarly, the UBT is also averaged over this time. Additionally, as the UBT profiling length exceeds the water depth, the data is cropped to

solely cover the water profile. From each bin an average is taken to produce an average backscatter profile which represents the backscatter of the entire run. Thus, giving us a representative LISST sampled suspended sediment concentration and the average backscatter profile of this run. The depth of the bed below the UBT changes over time as bedforms progress beneath the observation (figure 4.8 is a rather flat example). To obtain the velocities and backscatter at the same relative depths, the depths to produce profiles are normalised over the water column.

From this velocity profile an estimate of the relative importance of settling and suspending forces on the sediments can be made. This is quantified as the dimensionless Rouse parameter, which is calculated as follows:

$$P = \frac{w_f}{\kappa u_\tau} \tag{3.1}$$

w_f is the settling velocity [m/s] determined from Stoke's law of Settling, κ is the Von Kármán constant and u_τ is the shear velocity.
This Rouse parameter indicates the regime of sediment suspension (table 3.3).

Table 3.3: The Rouse parameter and corresponding regimes

Number	Regime
P<1	Full suspension
1<P<2.5	Incipient suspension
P>2.5	No suspension

Backscatter - SSC relation

To obtain the Sv-SSC relation, the time averaged SSC of the LISST is regressed against the time averaged backscatter amplitude at LISST sampling depth for each experiment. About 6 UBT bins are within the LISST sampling volume. For this relation only valid data is used, therefore, only runs with an average transmission value above 0.1 according to Sequoia Scientific (2022).

All backscatter and SSC runs from one experiment are regressed into one Sv-SSC relation. Thus, each regression embodies a sediment content depending backscatter-SSC relation. From backscatter profiles these regressed relations SSC profiles are derived.

On average, one non-dimensional cell height is 4.55 mm (33 cells over 15 cm water column on average). The suspend sediment transport flux is the multiplication of the velocity profile with the regressed SSC profile over the area a non-dimensional cell covers on average over the width of the flume (0.0054 m^2).

Threshold transmission value subjectivity

In order research to the subjectivity of the minimum transmission value Sequoia Scientific (2022) has chosen, the same processes of regressing the Sv-SSC relation for the experiments are repeated, but now with data including transmission values of 0.05 and higher. If these relations do not deviate much from the relations composed of data with average transmission values of 0.1 and higher, then there is reason to decrease the minimal transmission value to 0.05.

4 | Results

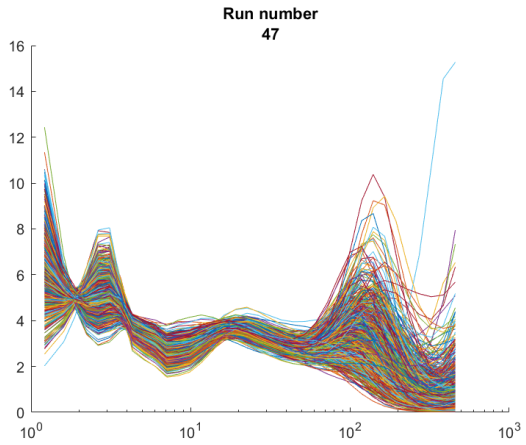

Figure 4.1: Instantaneous PSD profiles and subsequent volume concentrations for run 47. Each line represents one PSD recorded each second within a run. Run 47 has a bed composed of 95% medium sand and 5% coarse silt (d_{50} of 270 and 40 μm respectively.)

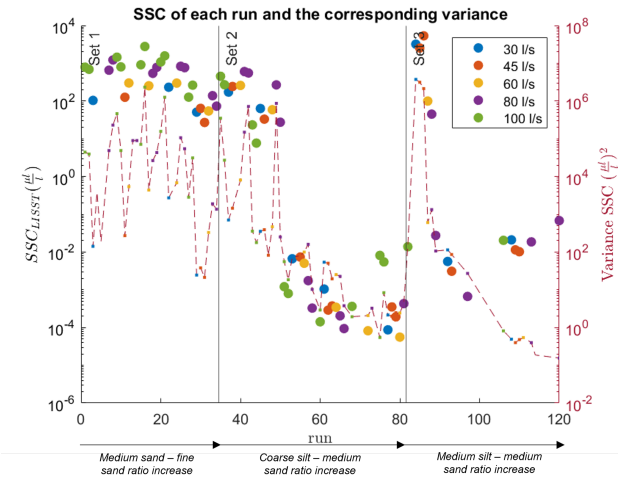

Figure 4.2: Recorded volumetric SSC for all runs. Indicated in colors are the discharges imposed on the run. The dotted line and smaller dots indicate the variance of each run. Note that the discharges in an experiment are not in the correct chronological order here. In this figure the discharges are given in the following order: 100, 30, 45, 60, 80 l/s.

4.1 LISST

4.1.1 SSC

The raw data recorded by the LISST represents time series of SSC and grain size distribution per run. This is the starting point of the results presented below.

The total suspended sediment content detected by the LISST increases with discharge in the first set and partially in the second. The SSC is also higher for set 1 compared to the others (figure 4.2). Set 2 and 3 show initially high SSC values, even though the water was refreshed between the two sets. When the water is refreshed, a lot of suspended fine sediments which trouble the water are removed. It is strange that the LISST records these high values compared to the following ones, because after refreshment the SSC was expected to be lower than the others. Especially for discharges of 30 litres per second. The SSC of the first three runs (30 l/s and 45 l/s) in set 3 are extraordinary high. These are the first medium silt runs after water refreshment. Runs 60 and 80 l/s maintain SSC values similar to sand runs, however, the 100 l/s run (first green dot in set 3) is in the low range again. For set 2, the observed SSC drops after a handful of runs from SSC values of a plausible magnitude to values 6 orders of magnitude below that. The elevated SSC values of the first runs in set 3 might be correct as visual observations clearly stated that the water turned into a milky white fluid once silt was added.

The variance in set 1 reacts proportional to discharge and is rather high compared to the majority of the runs in sets 2 and 3. When the water is turbid (last runs of sets 2 and 3), the variance drops about three orders below that of clear water. The first runs of set 3 show major variances. Analyzing the time series of these runs explains the cause of this variance (Run 84 is taken as an illustrative example, figure 4.4).

The recorded SSC varies massively when water conditions become turbid. Once the SSC rose to approximately 5000 $\frac{\mu l}{l}$, the recorded SSC started to fluctuate.

A closer look at figure 4.3 brings forward that in set 1 (blue), an increase of SSC with discharge is visible. The other two sets, however, show no pattern.

Set 1 shows little spread in suspended sediment content for each discharge, indicating similar recorded SSC for all sand-sand mixtures each discharge. Set 2 shows no pattern in discharge effect nor does it show any anomalies in SSC per discharge. Set 3, in contrast, does not show a pattern of discharge attenuated SSC increase nor does it provide any continuity of SSC for runs with the same discharge.

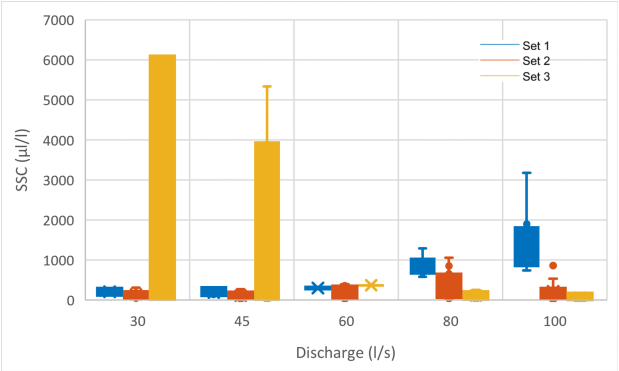

Figure 4.3: Each box plot indicates the variety of suspended sediment concentrations for the specified discharge within a set.

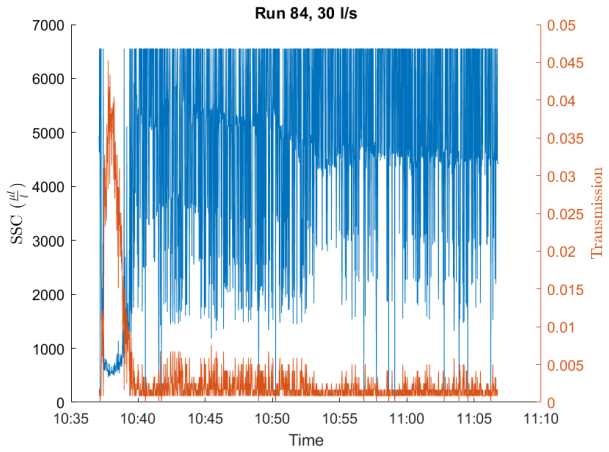

Figure 4.4: Time series of run 84. This is the first run of set 3 (medium silt after water refreshment). When the transmission drops, the SSC increases. This SSC has a large deviation in the order of 1000 $\frac{\mu l}{l}$. Other run examples are in the appendix (chapter 6)

4.1.2 Transmission parameter

The LISST laser beam travels through water from which the concentration is determined from the transmission, grain size and path length (eq. 2.1). So, lower transmission values would indicate higher suspended sediment concentrations. For the same sediment mixture, higher flow velocities give lower transmission values. Too low transmission values are obtained when the water is too turbid (above critical SSC in table 2.1). Sequoia Scientific (2022) therefore acknowledges a minimum transmission value of 0.1. This criterion is has not been achieved for most of the runs. Only one complete experiment and a hand full of runs have a transmission higher than 0.1 (figure 4.5). Besides the cluster of high transmission, three data points stand out: the first three runs of set 3. These transmission values are the lowest of the research while the first two

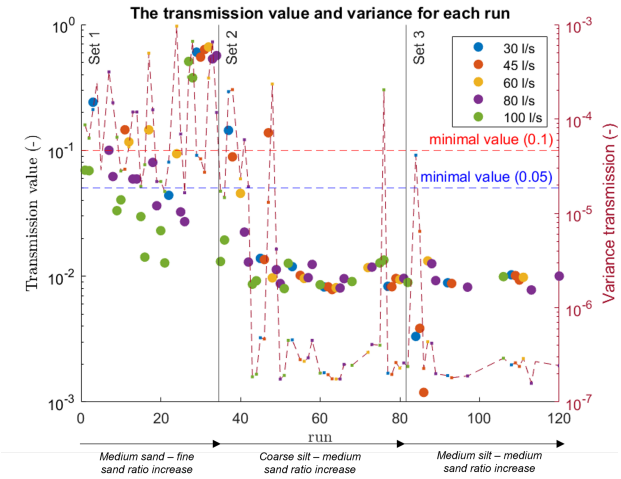

Figure 4.5: The mean transmission value for each run (large dots) with their respective variance (small dots and line, σ^2). In red and blue the present and proposed transmission threshold are projected respectively.

of these maintain a high variance. The high variance for these first two of three runs originate from the large change in transmission (e.g. run 84, figure 4.4) or show a continuous fluctuation in transmission in order of 0.007 (figure A.5). Run 86 (second red point) and the following runs do not deviate much. These runs all show a continuity of low transmission values. The bigger part of sets 2 and 3 show these low transmission values with low variance, all these low values occur a few runs after water refreshment.

The cluster of high transmission (last runs of set one) are identified as qualitatively good runs. The high variance in transmission and SSC are due to occasional peaks or due to trends. The gross of the occasional peaks, induced by sediment whirls, do not deviate much from the average SSC (7% deviation from the mean compared to the 10% of a poor run) or transmission (2% from the mean in contrast to 9% for a poor run). Only a couple of peaks deviate much more than that. These transmission and SSC peaks simultaneously show up inverse to each other (figure A.7). Trends show up over time where the SSC steadily rises to a plateau, while the transmission drops to a plateau (e.g. figure A.7). For the transmission this drop can be a multitude of three to nine times the average deviation around the moving average.

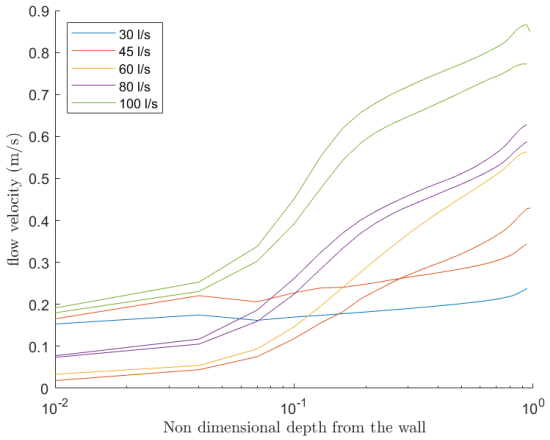

Figure 4.6: The mean velocity profiles of each 100% medium sand run on a non-dimensional depth scale from bed to water surface. Note that the non dimensional depth is on a logarithmic scale.

4.2 UBT

4.2.1 Velocity profile

The measured velocity profiles (figure 4.6) of each discharge closely resembles the expected velocities in table 3.2. The logarithmic velocity axis shows the logarithmic nature of the boundary layer. This shape is induced by the drag of the bed, decreasing the flow velocity towards the bed. One of the 45 l/s and the 60 l/s runs drop in the range of 0.02 m/s near the bed.

4.2.2 Rouse parameter

Table 4.1: Rouse parameter of each discharge for 100% medium sand experiment. "No" denotes the regime of No suspension and "Incip." denotes the Incipient suspension regime.

Q (l/s)	30	45	60	80	100
P	4.06	3.11	2.38	1.96	1.27
Regime	No	No	Incip.	Incip.	Incip

As a first indicator of the suspended sediment regime for each velocity, the Rouse parameter has been produced (table 4.1). No discharge of the 100 % medium sand experiment reached the full suspension phase. 60 Until 100 l/s are within the incipient suspension regime while 45 and 30 l/s should show no suspension. Video footage of the 100 l/s shows a lot of bed transport of rolling and saltating particles. Occasionally, a large whirl sweeps sediment high in suspension. The bed is rather flat. 80 l/s has little topography but quite some bed

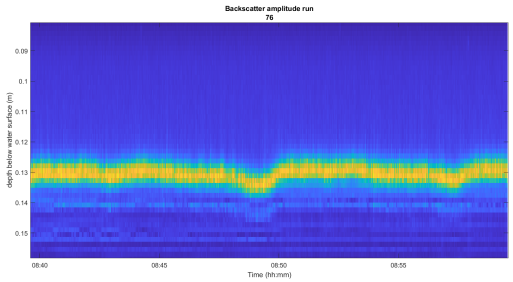

Figure 4.7: A time series of the backscatter profile. Orange and yellow colors around a depth of 13 cm indicate high backscatter amplitudes depicting the sediment bed.

motion. Particles roll and saltate while the occasional turbulent sweep suspends the particles. For 60 l/s, the smaller particles are in suspension for a moment when a reaching a certain location on the dune. There is a continuous rolling motion with some saltation. The 45 l/s run mainly shows a rolling behaviour. An occasional turbulent sweep over dunes causes the sediments to saltate, yet the particles seldom go into suspension. Unfortunately, there is no video coverage of the 30 l/s run.

4.2.3 Backscatter profile

The backscatter amplitude (Sv) time series, an example presented in figure 4.7, show high backscatter amplitudes at the bed as this hard surface reflects echoes very well. The backscatter amplitude at the bed surface and below are omitted to only capture Sv for the water column. From this time series also dune formation and propagation are visible. Another example of an uncut backscatter time series profile with clear dune propagation is given in the Appendix (figure A.8)

The average backscatter intensity within the column, figure 4.8, is highly dependent on discharge. The profile average backscatter amplitude has distinct values for each discharge. Noticeable is the abrupt drop of backscatter in set 3. The fine silt seems to have a property to relatively attenuate the backscatter amplitude. Still, the unambiguous discharge dependency is visible.

The backscatter amplitude profile over normalised depth (figure 4.9) shows a general trend of Sv increase towards the bottom and also an increase of backscatter with the discharge.

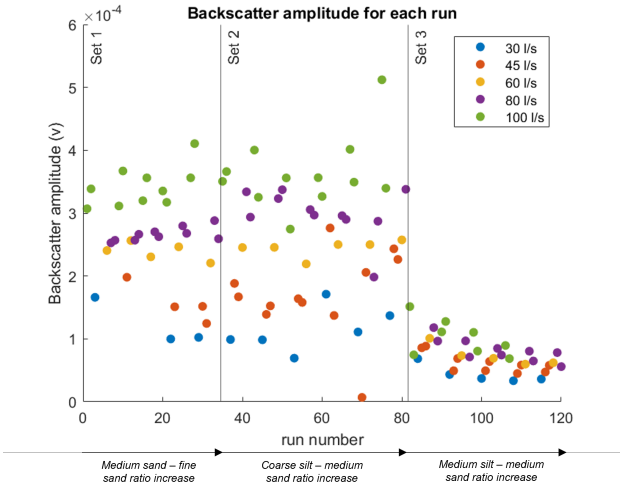

Figure 4.8: The average backscatter amplitude for each run. An unmistakable discharge/velocity dependency emerges.

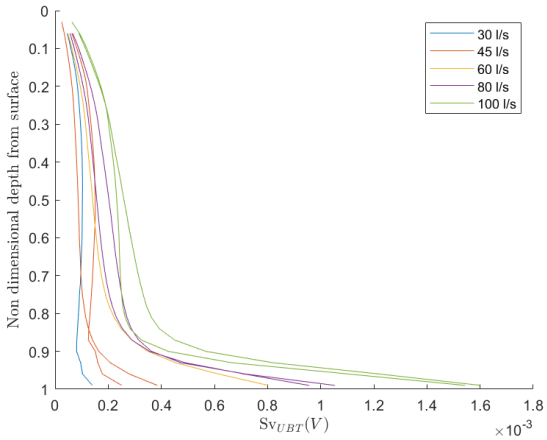

Figure 4.9: Non dimensional time averaged backscatter profile of the experiment with transmission values higher than 0.1

4.3 Backscatter-SSC relation

From found results on the quality of sampling, the runs including silt are omitted from any further analysis as these samples are corrupted. Based upon the transmission values exceeding 0.1 only the 100% medium sand experiment meets this specification (yellow line in figure 4.10) as the average transmission value for this experiment is approximately 0.5. The only experiments with at least two runs with a transmission value above 0.05 are 100% fine sand and 80% fine sand - 20% medium sand. The 80-20% composition only has two points, therefore shows a perfect line. This is also the reason it is dropped out of the comparison. 100% Fine sand shows a lot of scatter. From these 5 points the Sv-SSC relation for fine sand emerges. Expected was a similar trend visible for

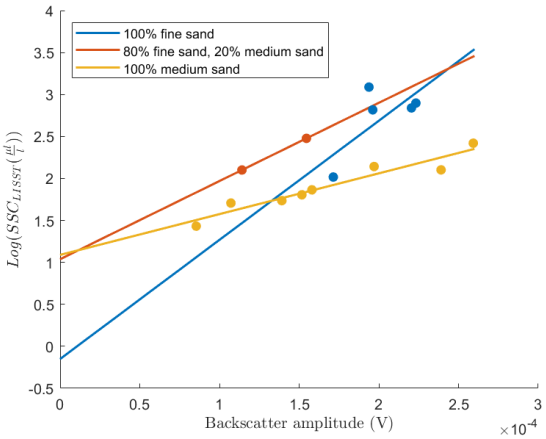

Figure 4.10: Backscatter amplitude - SSC relation for experiments with transmission values above 0.05. The 100% medium sand is the only experiment with transmission values above 0.1 and therefore is leading in comparison.

both sediment compositions, however, this relation for fine sand diverges significantly from the medium sand experiment relation. Also, due to the noisy nature of the fine sand relation, this data cannot be trusted.

SSC flux

The suspended sediment flux is a product of the flow velocity, average surface area of a normalised depth cell and regression derived SSC (figure 4.11). Since the regression is only valid for the 100% medium sand experiment, the flux is only determined for these runs. The shape of the flux over depth looks very similar to figure 4.9, as the backscatter amplitude is highest near the bottom. The flux of one of the 45 l/s runs drops around a non dimensional depth of 0.93. This has partially to do with the low backscatter amplitude and partially with the drop in flow velocity (figure 4.6). The figure is cropped to a maximum SSC flux of 0.0033 cubic metres per second. This discharge is equal to a recording of a non-dimensional cell, filled solely with water flowing at the specified velocity for the maximum discharge (100 l/s). A volumetric sediment flux equal to 3.3 l/s in a non-dimensional depth cell is impossible, as in that case, the this cell transports only sediment, not even any water anymore. The flux is fully saturated with sediment. Surpassing this flux as the green lines do indicate a larger volume sand passing than volumetrically possible. The vertical line in figure 4.11 indicates the same process of non dimensional cell saturation, but now for 30 l/s. The 30 l/s flux is almost 5 orders of magnitude

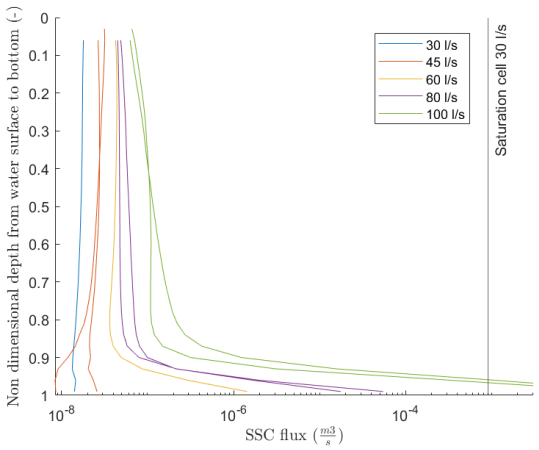

Figure 4.11: SSC flux profile derived from backscatter amplitude and flow velocity. The SSC-Sv relation is extrapolated from the experiment with transmission higher than 0.1. The 30 l/s cell saturation line is a threshold line when one non dimensional cell only transports sediment and no water in case of a 30 l/s run.

lower than this cell saturation limit.

This brings forward that the sediment flux of the 100 l/s run is too high near the bottom. The other sediment fluxes do not show any problematically high values.

5 | Discussion

5.0.1 Interpretation

So far found is that the LISST underestimates the suspended sediment concentration significantly once the water approaches the milky white state which can be addressed to silt suspension (figure 4.2). The transmission values drop below 0.1 (figure 4.5), the corollary being that the water is simply too turbid for the laser beam to pass through. The relative low transmission values for the majority of the runs in the first set are attributed to residual clay particles from previous experiments (van Wijk, 2021). The amount of fine material differs each run (figure A.2), but almost always passes the maximum SSC for the smallest particles with a transmission threshold of 0.3 (table 2.1, eq. 2.1). The last runs are the only ones with no finest sediments in suspension and therefore have such a good quality.
High variances in SSC and transmission are either due to trends with a multitude of the deviation from the moving average or due to large scattering. For the runs with low transmission (the major part of sets 2 and 3), the variance of transmission and SSC is low. This is caused by the fact that the LISST is unable to record any valid SSC data nor is able to correctly measure the transmission.
All in all, the LISST transmission threshold of 0.1 seems to be valid. For runs with a transmission between 0.05 and 0.1 the SSC shows noise similar to the runs with a transmission of 0.1 and higher. Furthermore, the Sv-SSC relation is also fairly different to the reference experiment, plus there is a lot of scatter (figure 4.10). These two observations indicate bias in SSC determination for samples with a transmission value between 0.05 and 0.1. The UB-Lab 2C has mainly issues from backscatter attenuation (figure 4.8). Once the particle size becomes too small (medium silt: $d_{50} \approx 18\mu m$), the received backscatter is considerably attenuated.

The rest of this chapter devotes attention to similar observed problems in other studies and some proposed methodological changes are given regarding the setup to prevent these problems to arise in future experiments or field campaigns.

5.1 LISST

In a field study inside a water way of a hydropower plant, Felix et al. (2018) found for a fixed SSC, the turbidity would decrease with particle size. The median particle size was approximately 15 µm, similar to the experiment conducted in our research. This emphasizes the problem of optic sediment determination for finer fractions that present research stumbled upon. They also found an LISST-100X determined SSC overestimation of 79% . This was mainly caused by effects of highly non-spherical particle shapes and perchance to flocculation.

Felix et al. (2018) recommend in-situ SSC determination for silt to be recorded by both a LISST and a CFDM (Coriolis Flow and Density Meter) for a wide range of concentrations (1 mg/l to 13.5 g/l). Once the transmission limit of the LISST is reached, the CFDM captures these higher SSC as the relative error drops with SSC. This CFDM determines the suspended sediment content on the density difference between clear water and the water with suspended sediments. The water flows through pipes that vibrate at their natural frequency. The natural frequency decreases with the pipe mass. From the density of the particle and the frequency difference between clear water and sediment-laden water the total SSC can be derived (Holcomb & Outcalt, 1998). The downside of this method is the lack of information regarding the particle sizes. As only the flow density can be derived with the CFDM, the PSD is disregarded. Therefore, overlooking valuable information regarding which sediment sizes are in transport.

Something that could occur resolving the SSC and PSD is bias due to extraordinary scattering from irregular shaped particles. Not only do irregular particles have a broader scattering range, the smallest irregular particles scatter more light than similar spherical shaped ones (Czuba et al., 2014). Since the medium silt used is rather small, any irregularities on the particle shape would lead to extra scattering and therefore create bias in the PSD. On the LISST an irregular particle shape model can be applied during SSC recording to account for the additional irregularities induced scatter. However, this model was not applied during all experiments. Even more, it is unknown which runs do have this model applied. So, it is uncertain which experiments are biased due to the irregular particle model absence.

The sediment composition itself is also of major importance. Particles smaller than 20 µm affect the scattering pattern (Andrews et al., 2010).

This brings forward the problem of multiple scattering in turbid conditions present research is presented with. Due to the silt smaller than 20 µm, scattering would lead to signal dissipation as the signal scatters over a wider range for multiple times. Thus, a drop of transmission also indicates PSD bias from multiple backscatter such as the tailing.

Zhao et al. (2018) encountered SSC underestimation of oil droplets between 8 and 28% for a transmission value of 0.3. This study also found the SSC_{max} for a transmission value of 0.3 to be achieved at 50% the proposed SSC. The out-of-range particle sizes were not stored in the nearest grain size bin as Agrawal & Pottsmith (2000) proposed, but were added to the lower 2 and higher 8 bins. For the research of Zhao et al. (2018), it should be noted that the partitioning of grain sizes to the largest 8 bins applies for particles larger than 1000 µm. For particles with a size of 500 µm (more probable in present research), these extra large particles were added to the nearest 4 bins. From these bins, the largest bin felt the most pronounced concentration addition.

This addition spread may explain the tails at the end of the instantaneous particle size distributions to be longer than 1 bin in case the irregular particle shape model was not applied.

It is important to be certain that the calibration data (LISST data) is correctly observed, but also is unambiguous. In the study of Sehgal et al. (ript), proposed a generic calibration approach to estimate the Suspended Particular Matter Concentration (SPMC) from turbidity, SPM particle size, carbon content and colour (based on the Munsell Value). This brings forward the issue of bias imposed by each of these variables. In this lab experiment, no carbon content/organic matter was introduced in the system and the particle size and turbidity are known. However, the colour is an issue that needs to be addressed when measuring the SSC of different sediment mixtures as the generic calibration approach provides a slight improvement compared to local calibration.

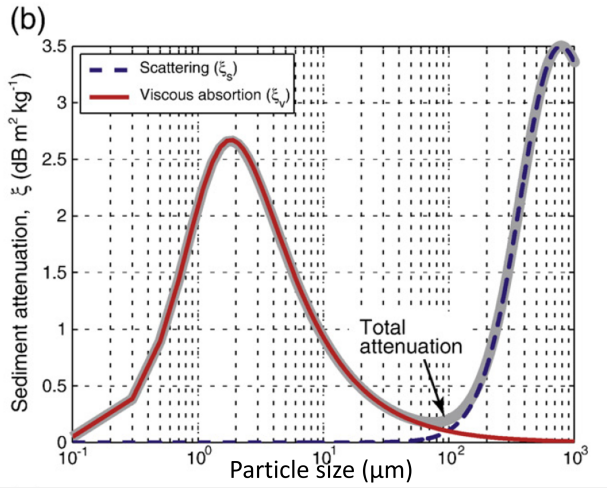

Figure 5.1: After Ha et al. (2011), the total backscatter attenuation depends on the scattering (blue line) and viscous absorption (red line). These two depend both on the scatter grain size.

5.2 UBT

5.2.1 Acoustic attenuation medium silt

Previously mentioned, the backscatter amplitude is severely attenuated once medium silt was introduced in the bed (figure 4.8).

Acoustic attenuation in water is determined by temperature, pressure, salinity, frequency and the suspended sediment properties, e.g., size, shape, mineralogy and SSC (Urick, 1983; Richards et al., 1996). These factors can be categorized into two classes: water attenuation (α_w) and suspended sediment attenuation (α_s). The temperature, pressure, salinity and frequency regulate the attenuation by water, while the frequency and sediment properties determine the suspended sediment attenuation. α_s in turn depends on absorption components ξ_s (scattering) and ξ_v (viscous absorption) (Richards et al., 1996):

$$\alpha_s = \frac{1}{R}\int_0^R (\xi_s + \xi_v) SSC(r) dr \qquad (5.1)$$

R is the sensing range, r is the sub-distance from the emitter and SSC is the suspended sediment content. The influence of scattering dominates from grain sizes larger than 100 µm and is most pronounced around 800 µm (figure 5.1). Viscous absorption however, is most pronounced around 2 µm. Viscous absorption is the energy loss in heat from acoustic wave induced particle motion.

The attenuation curves are less pronounced for the UBT frequencies as for the 1.5 MHz SonTek (figure 5.2).

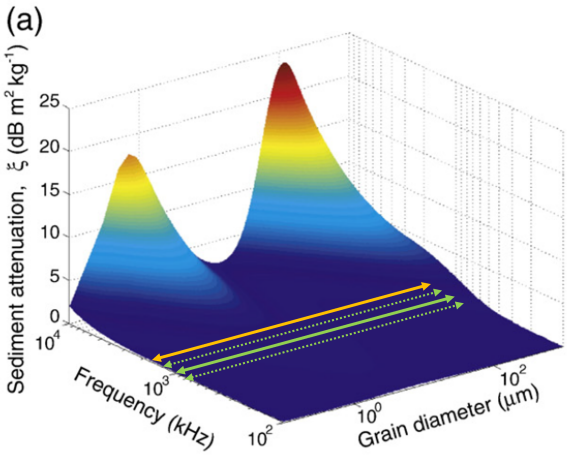

Figure 5.2: The orange arrow displays the emitted frequency of the SonTek (1.5 MHz). The range of the UB-Lab 2C is indicated with the dotted green lines (0.8 - 1.2 MHz), the solid green line is the emitted UBT frequency (1.0 MHz). The attenuation curves in figure 5.1 are on the orange frequency line. Figure retrieved from Ha et al. (2011).

However, for a frequency of 1 MHz and higher the viscous absorption is far more important than scattering in silt-laden water (Ha et al., 2011) and would already lead to 30% energy loss for concentrations of 0.5 grams clay ($2\mu m$) a litre.

In the "hydropower plant study" of Felix et al. (2018), the acoustic attenuation decreased with sediment size. They use the attenuation as an indication of SSC, depending on the grain size.

In determining the viscous absorption of glass beads ($d_{50} \approx 40\mu m$) suspended in a water column, Brown et al. (1998) found the reverberation time to decrease with concentration. The reverberation time is the time it takes for an acoustic pulse to drop 60 dB. This acoustic loss time is also dependent on the acoustic frequency, as the reverberation time drops with frequency (in this experiment ranges from 50 to 150 kHz). These frequencies are an order of magnitude lower than the UBT, thus, the attenuation Brown et al. (1998) found is less pronounced than in present study (figure 5.2).

From the aforementioned studies the conclusion can be made that the dissipation of acoustic intensity is something that already occurs in circumstances less extreme than present study has dealt with. Thus, these processes affecting the backscatter amplitude are genuinely important.

The backscatter attenuation components ξ_w and ξ_s can be derived indirectly with elaborate calibration. If the experiment is repeated with the same experimental setup, only now excluding all sediments, ξ_w is obtained, as this is the only attenuation of influence. The difference between total attenuation of a clear water experiment and sediment-laden water gives ξ_s. For each sediment mixture, there is a specific attenuation that can be used for SSC determination.
In a follow up study, ξ_v and ξ_s have to be resolved for each grain size composition.

5.2.2 SSC profile heterogeneity

Experimental setups proposed for backscatter attenuation determination (Ha et al., 2011; Thorne et al., 1991; Thorne & Hanes, 2002) use stirrers to suspend sediments and grain sizes homogeneously over the water column. Field conditions and present lab research, in contrast, contain vertically heterogeneous grain size distributions (fining upwards). Introducing a attenuation coefficient only depending on grain size overlooks the depth variability of grain sizes. To correctly incorporate the attenuation of a profile into a Sv-SSC model, the heterogeneity of the grain size distribution needs to be measured and parameterized to include all physical influences individually. This in turn leads to a better understanding and a completer vision of suspended sediment transport.

5.3 SSC flux

The derived SSC flux is way too high in case of the 100 l/s run. It surpasses the maximal possible flux (a flux of only sand, no water) about 20 times.
The main constituents of the flux are the flow velocity, the backscatter profiles and the Sv-SSC relation. The velocity profile (figure 4.6) of this run looks perfectly normal, a logarithmic velocity profile (Klewicki et al., 2009). The backscatter profile (figure 4.9) looks reasonably well too. Both profiles show an increase with discharge. Therefore, these two constituents can be excluded from having effect on the extreme flux. Ergo, the Sv-SSC relation needs to be assessed in detail.

The trend in SSC increase with backscatter amplitude is fairly strong (figure 4.10, R^2 of 0.921). This relation is based upon the average backscatter of the UBT bins at the height of the LISST sampling volume. The recorded SSC values at LISST depth are not dramatically high for these runs, neither are the backscatter

amplitudes. However, for the entirety of the profile, the backscatter amplitude does increase considerably near the bed. These amplitudes are far beyond the range of the interpolated backscatter - SSC relation. Extrapolating this relation for these backscatter values brings unrealistic values. Therefore, the Sv-SSC relation is not compatible for all the flow regimes and depths.
The produced sediment flux does produce proper values above the relative depth of 0.8 or 0.9. Therefore, the flux is still usable for near water surface suspended transport.

5.4 Research application

A suggestion to increase the data quality of the LISST in turbid regions would be to increase the transmission value. Equation 2.1 shows the dependency of the maximum observable concentration to the transmission value and path length. If the path length is shortened, the SSC range increases. Sequoia Scientific provides a module in line with the suggested solution: the Path Reduction Module. The PRM reduces the path length to 5 mm instead of the original 25 mm. This results in maximum observable SSCs 5 times higher than without the PRM.

Another suggestion would be to dilute the water sample to increase the transmission value. Injecting the sampled water volume from a certain depth into a fixed volume of water dilutes the SSC with a known ratio. Measuring the diluted sampling volume gives the same grain size composition, only with their respective concentrations a ratio lower than in field. The original SSC can be derived from the diluted SSC and the dilution ratio. If this process can be executed uninterruptedly, a continuous set of SSC data is collected which in turn can be used to produce the backscatter-SSC relation.

Considering the suggestions of diluting and shortening the laser path length, a proposed experimental setup would be to continuously pump water from multiple depths through little hoses. These hoses should be connected to a LISST each, with the proviso that these LISSTs are equipped with either a shortened sampling volume or a dilution system. Now the LISST can analyse the pumped water volumes correctly on SSC at the same moment the UBT records the backscatter amplitude.

The most trustworthy method still is sampling suspended sediment, measure the mass by dry weighing. The major downside is the labour intensive and time consuming process. However, this method can be used to validate the LISST or calibrate the backscatter-SSC relation. Another advantage is that this method still allows PSD determination as the particles are conserved.

6 | Conclusion

From the lab experiments, a few important issues are concluded.

Smaller sediment particles severely affects optical measuring devices through transmission reduction, so does silt. In this experiment the suspended silt content was too high, reducing the transmission below the thresholds of 0.3 and 0.1. This was also the case for the majority of the sand runs. These sand runs are most probably corrupted with finer residual sediments of previous experiments. From the data of the runs which are well above the threshold, a solid logarithmic relation between the backscatter intensity and suspended sediment content was found. The applicable range of SSC in this relation was surpassed near the sediment bed at high discharge. Near the bed absurdly high sediment fluxes were found exceeding the physically possible maximum flux. Lowering the threshold transmission value of 0.1 of 0.3 to 0.05 is not viable. The Sv-SSC relation differs from the valid relation and is filled with noise. Therefore, in case the transmission value drops below the set limit (Sequoia Scientific, 2022), the data should be treated as faulty and cannot be used in any further analysis.

It is recommended to adapt some changes to the LISST setup in order to collect data more accurately in the future:

It is wise to either reduce the path length as this a variable that would increase the maximum observable SSC (equation 2.1), or dilute the SSC sample by a fixed volume. The mass and particle size distribution of the sample remain the same, only the concentration decreases with a fixed value which can be easily converted back to the in-situ samples. The Sequoia company provides both these adaptations. This way sensible SSC values can be collected under turbid circumstances.

Silt also corrupted the UB-Lab 2C data. Due to viscous absorption, the backscatter amplitude dropped significantly. The backscatter amplitude dropped, however, in a relative sense: the backscatter amplitude still followed discharge/SSC but were in general lower and closer to each other. The UBT is therefore able to record sensible data.

To produce a relation between Sv and SSC is achievable if you consider this grain size dependent attenuation and capitalize on this physics through an improved setup and calibration:

If the SSC is sampled near the surface and at bed depth, the sediment induced attenuation can be accounted for, thus, incorporating the grain size dependent attenuation into the Sv-SSC relation. In this manner also the vertical particle size heterogeneity can be taken into account to improve the understanding of sediment transport.

In conclusion, the effect of sediment composition and suspended sediment concentration on suspended sediment transport determination in a lab setting is mainly that the finer sediments overwhelm the optical sediment content monitor (LISST) and attenuate the PSD. The UBT records attenuated data which can be attributed to viscous absorption from medium silt particles. Some minor adjustments in the device setup would give much more confidence in suspended sediment transport determination. SSC determination based on backscatter is promising if the SSC samples are calibrated at two depths to counter attenuation. Furthermore, if modules are added to the LISST, which increase the maximum observable concentration, the high concentrations of suspended silt would be recorded correctly.

Acknowledgements

I would like to thank my supervisors Iris Niesten and Ton Hoitink, as they shared their wide experience within the subject of fluid mechanics and sediment transport with me to keep this thesis clinical and concise. They guided me a lot with providing theoretical background and gave important advice regarding conceptualising the approach of tackling the faced problem. In special I would like to acknowledge Iris, who assisted me with translating data analysis ideas into code when my MATLAB skills reached their limit and gave advice during weekly meetings.

Many regards to Sjoukje de Lange, who not only contributed in the orientation phase to come to a topic and a experimental setup, but also provided some interesting literature in earlier phases to sharpen this thesis.

I would also like to thank Sanne van de Veen, sister in the experiment. She, Iris and Sjoukje spent many hours in the lab running the experiments, shoveling tonnes of sediments and giving structure to the data sets.

Vera Smits helped me through moments of adversity. I am grateful for the conversations we've had.

Also a big thank you to David Boelee and Pieter Hazenberg, research technicians at the Wageningen University & Research in the Kraijenhoff van de Leur Laboratory for Water and Sediment dynamics, because of their keen vision on practically dimensioning the experiment, helping us during the experiments and managing the lab.

Bibliography

Agrawal, Y., Whitmire, A., Mikkelsen, O., and Pottsmith, H. C. Light scattering by random shaped particles and consequences on measuring suspended sediments by laser diffraction. *Journal of Geophysical Research*, 113, 2008.

Agrawal, Y. C. and Pottsmith, H. C. Laser diffraction particle sizing in stress. *Continental Shelf Research*, 14, pp. 1101–1121, 1994.

Agrawal, Y. C. and Pottsmith, H. C. Instruments for particle size and settling velocity observations in sediment transport. *Marine Geology*, 168, pp. 89–114, 2000.

Agrawal, Y. C. and Traykovski, P. Particles in the bottom boundary layer: Concentration and size dynamics through events. *Journal of Geophysical Resources*, 106, pp. 9533–9542, 2001.

Andrews, S., Nover, D., and S.G., S. Using laser diffraction data to obtain accurate particle size distributions: The role of particle composition. *Limology and Oceanography Methods*, 8, pp. 507–526, 2010.

Andrews, S. W., Nover, D. M., Reuter, J. E., and Schladow, S. G. Limitations of laser diffraction for measuring fine particles in oligotrophic systems: Pitfalls and potential solutions. *Water Resources Research*, 47, 2011.

Baas, J. A flume study on the development and equilibrium morphology of current ripples in very fine sand. *Sedimentology*, 41, pp. 185–209, 1994.

Baas, J., Davies, A., and Malarkey, J. Bedform development in mixed sand-mud: The contrasting role of cohesive forces in flow and bed. *Geomorphology*, 182, pp. 19–32, 2013.

Bartzke, G., Bryana, K., Pilditch, C., and Huhn, K. On the stabilizing influence of silt on sand beds. *Journal of Sedimentary Research*, 83, 2013.

Betteridge, K., Thorne, P., and Cooke, R. Calibrating multi-frequency acoustic backscatter systems for studying near-bed suspended sediment transport processes. *Continental Shelf Research*, 28, pp. 227–235, 2008.

Brown, N., Leighton, T., Richards, S., and Heatherstraw, A. Measurement of viscous sound absorption at 50–150 khz in a model turbid environment. *The Journal of the Acoustical Society of America*, 104, 1998.

Czuba, J., Straub, T., Curran, C., Landers, M., and M.M., D. Comparison of fluvial suspended-sediment concentrations and particle-size distributions measured with in-stream laser diffraction and in physical samples. *Water Resources Research*, 51, pp. 320–340, 2014.

Davis, B. A guide to the proper selection and use of federally approved sediment and water-quality sampler, 2005.

Doppler, C. *"Uber das farbige Licht der Doppelsterne und einiger anderer Gestirne des Himmels*. F. J. STUDNICKA, 1842.

Edwars, T. and Glysson, G. *Field methods for measurement of fluvial sediment*. Reston, 1999.

Felix, D., Albayrak, I., and Boes, R. In-situ investigation on real-time suspended sediment measurement techniques: Turbidimetry, acoustic attenuation, laser diffraction (LISST) and vibrating tube densimetry. *International Journal of Sediment Research*, 33, pp. 3–17, 2018.

Fischer, S. Development of an ultrasonic instrumentation for fluid velocity measurement beyond the Nyquist limit by a spectral approach. *HAL archives*, 1, 2004.

Gartner, J. W., Cheng, R. T., Wang, P. F., and Richter, K. Laboratory and field evaluations of LISST-100 instrument for suspended particle size determinations. *Marine Geology*, 175, pp. 199–219, 2001.

Gray, J., Glysson, D., and Edwards, T. *Suspended-sediment samplers and sampling methods*. Reston, 2008.

Ha, H., Maa, J.-Y., Park, K., and Kim, Y. Estimation of high-resolution sediment concentration profiles in bottom boundary layer using pulse-coherent acoustic doppler current profilers. *Marine Geology*, 279, pp. 199–209, 2011.

Heus, T. Calibration of acoustic backscatter. Master's thesis, Wageningen University & Research, 2020.

Hoitink, A., Wang, Z., Vermeulen, B., Huismans, Y., and Kästner, K. Tidal controls on river delta morphology. *Nature Geoscience*, 10, 2017.

Holcomb, C. and Outcalt, S. A theoretically-based calibration and evaluation procedure for vibrating-tube densimeters. *Fluid Phase Equilibria*, 150, pp. 815–827, 1998.

Klewicki, J., Fife, P., and Wei, T. On the logarithmic mean profile. *Journal of Fluid Mechanics*, 638, pp. 73–93, 2009.

Mikkelsen, O. and Pejrup, M. In situ particle size spectra and density of particle aggregates in a dredging plume. *Marine Geology*, 170, pp. 443–459, 2000.

Mikkelsen, O. and Pejrup, M. The use of a lisst-100 laser particle sizer for in-situ estimates of floc size, density and settling velocity. *Geo-Marine Letters*, 20, pp. 187–195, 2001.

Mikkelsen, O. A., Hill, P., Milligan, T. G., and Chant, R. J. In situ particle size distributions and volume concentrations from a LISST-100 laser particle sizer and a digital floc camera. *Continental Shelf Research*, 25, pp. 1959–1978, 2005.

Naqshband, S. and Hoitink, A. Scale-dependent evanescence of river dunes during discharge extremes. *Geophysical Research Letters*, 47, 2020.

Naqshband, S., van Duin, O., Ribberink, J., and Hulscher, S. Modeling river dune development and dune transition to upper stage plane bed. *Earth Surface Processes and Landforms*, 41, pp. 323–335, 2016.

Reynolds, R. A., Stramski, D., Wright, V. M., and Woźniak, S. B. Measurements and characterization of particle size distributions in coastal waters. *Journal of Geophicical Research*, 115, 2010.

Richards, S., Heatherstraw, A., and Thorne, P. The effect of suspended particulate matter on sound attenuation in seawater. *The Journal of the Acoustical Society of America*, 100, pp. 1447 – 1450, 1996.

Sassi, M., Hoitink, A., and Vermeulen, B. Impact of sound attenuation by suspended sediment on ADCP backscatter calibrations. *water resourches research*, 48(9), 2012.

Sehgal, D., Martínez-Carreras, N., Hissler, C., Bense, V., and Hoitink, A. A generic relation between turbidity, suspended particulate matter concentration and sediment characteristics. *Journal of Geographical Research*, Accepted Manuscript.

Sequoia Scientific, I. *LISST-200X Particle Size Analyzer*. Sequoia Scientific, Inc, 2022.

Shannon, C. Communication in the presence of noise. *Proceedings of the Institute of Radio Engineers*, 37(1), pp. 10–21, 1949.

Thorne, P. and Hanes, D. A review of acoustic measurement of small-scale sediment processes. *Continental Shelf Research*, 22, pp. 603–632, 2002.

Thorne, P., Vincent, C., Hardcastle, P., Rehman, S., and Pearson, N. Measuring suspended sediment concentrations using acoustic backscatter devices. *Marine Geology*, 98, pp. 7–16, 1991.

UBERTONE. ADVP Measurement Principle User manual, 2019.

Urick, R. *Principles of Underwater Sound*. McGraw-Hill, 1983.

van Ledden, M., van Kesteren, W., and Winterwerp, J. A conceptual framework for the erosion behaviour of sand–mud mixtures. *Continental Shelf Research*, 24, pp. 1–11, 2004.

Van Rijn, L. Erodibility of Mud–Sand Bed Mixtures. *Journal of Hydraulic Engineering*, 146(1), pp. 1–19, 2020.

van Wijk, J. Linking hydraulic roughness from dunes to detailed flow processes. Master's thesis, Wageningen University & Research, 2021.

Yao, P., Su, M., Wang, Z. van Rijn, L., Stive, M., Xu, C., and Chen, Y. Erosion behavior of sand-silt mixtures: Revisiting the erosion threshold. *Water Resources Research*, 58, 2022.

Zhao, L., Boufadel, M., King, T., Robinson, B., Conmy, R., and Lee, K. Impact of particle concentration and out-of-range sizes on the measurements of the lisst. *Measurement Science and Technology*, 9, 2018.

A | Additional figures

Table A.1: The grain size distribution of each sediment

Sample Name	medium silt	coarse silt	fine sand	medium sand
d (0.1) µ	2.43	3.658	106.781	182.403
d (0.5) µ	17.818	39.111	179.343	270.096
d (0.9) µ	46.265	133.749	298.766	399.655

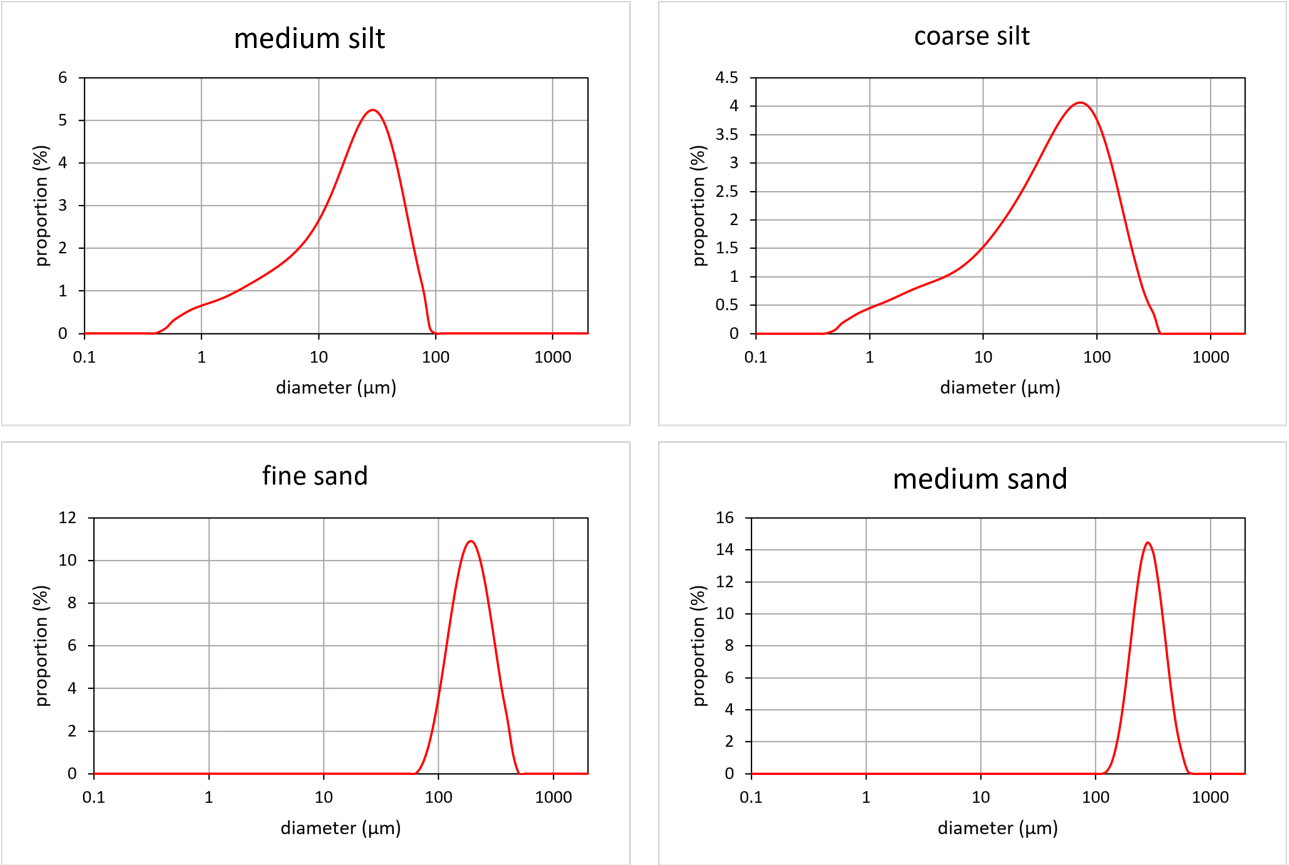

Figure A.1: The grain size distributions of the used sediments

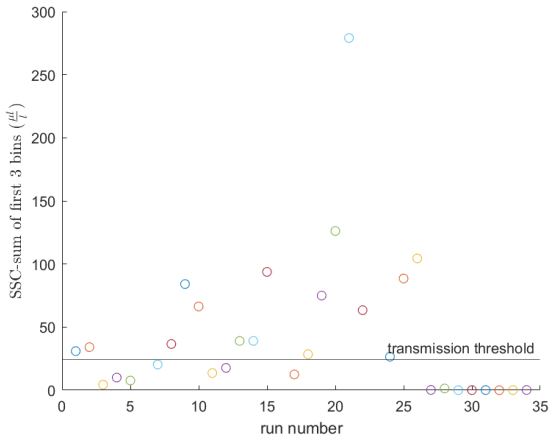

Figure A.2: The sum of suspended sediment content of the first three PSD bins. On average these bins represent a grain size of 1.5 µm. The threshold line indicates whether the tolerable SSC of these grain sizes surpass the SSC based on the transmission threshold of 0.3. Clear is the absence of finest sediments in the last runs of the first experiment.

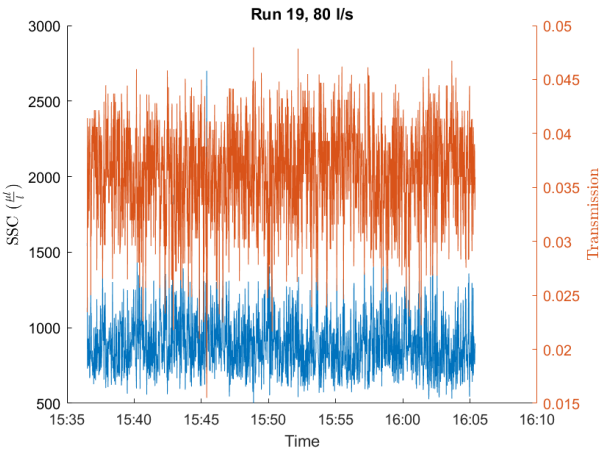

Figure A.3: Time series of run 19. This is one of the runs with a transmission value just below 0.05, illustrating the large variance in figure 4.5. The deviation is in order of 100 $\frac{\mu l}{l}$

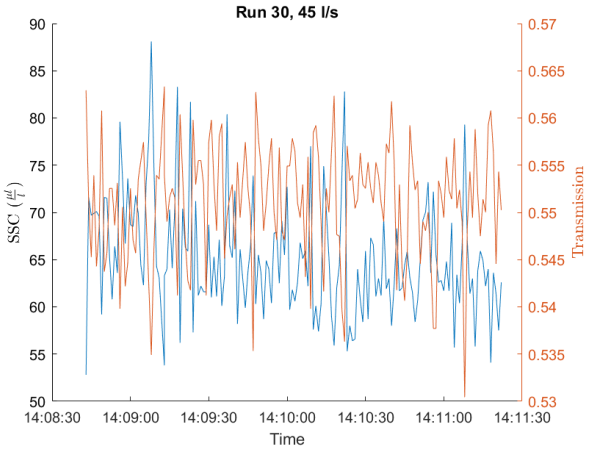

Figure A.4: Time series of run 30. This is one of the runs from the cluster with a high transmission. The deviation of is in order of 10 $\frac{\mu l}{l}$

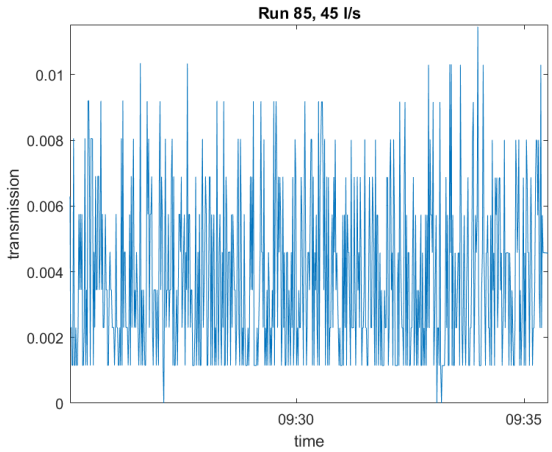

Figure A.5: Transmission of run 85

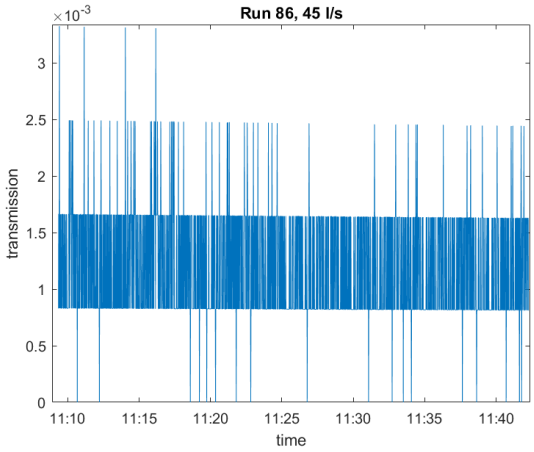

Figure A.6: Transmission of run 86

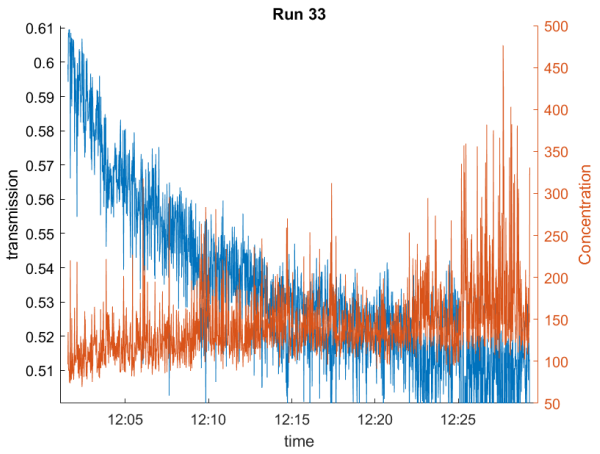

Figure A.7: Transmission and concentration of run 33 showing trends in opposite direction between the two.

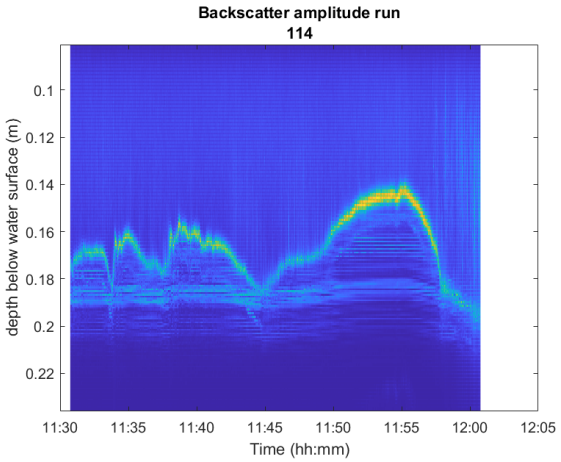

Figure A.8: Uncut backscatter time series of run 114. Notice dune propagation below the UBT.